Optimization of the Countercurrent Moving-Bed Chromatographic Separator

Barry B. Fish, Robert W. Carr, and Rutherford Aris
Dept. of Chemical Engineering and Materials Science, University of Minnesota, Minneapolis, MN 55455

A dispersionless, adsorption equilibrium, plug-flow model of a countercurrent moving-bed chromatographic separator operating at steady state is investigated. The flux of the constituents of a binary mixture is examined via concentration-phase plane plots, which reveal a complex behavior depending on a parameter σ, the ratio of solid- and fluid-phase flow of the mobile phase. When the model is modified by incorporating finite mass-transfer rates, axial concentration profiles exhibit behavior that is characteristic of experimental observations, rather than the predictions of the ideal model. Numerical simulations with the finite mass-transfer model reveal an optimum operating condition.

Introduction

The countercurrent moving-bed chromatographic separator (CMCS) is a column, in which a granular solid flows counter to an inert carrier fluid and into which the mixture to be separated is continuously introduced at an arbitrary axial position. Differences in adsorption affinity of the solid for the constituents of the mixture lead to a chromatographic separation. Theoretical and experimental progress on countercurrent moving-bed separations has received several reviews during the past decade (de Rosset et al., 1981; Ruthven, 1984; Barker and Ganetsos, 1987, 1989).

Analysis of a steady-state, isothermal, plug-flow, countercurrent, moving-bed separator incorporating the Langmuir isotherm has revealed that the behavior of the system depends critically on a parameter, σ, the ratio of the flux of adsorbed species to the flux of fluid-phase species, at low concentrations where the isotherm is approximately linear (Altshuller et al., 1987). An analysis of the behavior of a single adsorbate obeying a Langmuir isotherm has shown that at higher concentrations there is a complex interplay between σ and fluid-phase concentration that strongly influences the axial concentration distribution in the CMCS (Fish et al., 1989). This communication extends the analysis to binary mixtures, showing that while a dispersionless model is capable of explaining the principal features observed experimentally (Fish et al., 1989), it is necessary for the model to include a mechanism that produces axial dispersion for a full accounting of the observations. Furthermore, the analysis reveals that there is an optimum separator length maximizing productivity while maintaining a good separation.

A dispersionless, adsorption equilibrium (Langmuir isotherm) model which shows qualitatively how components move either up or down the column is first presented. A closer examination of binary separations is then approached with the aid of dimensionless concentration-phase plane plots. This permits a detailed picture of how the distribution of the components along the CMCS depends on σ and fluid-phase composition. Although the dispersionless, adsorption equilibrium model provides a convenient means to understand the principal features of the CMCS, the axial concentration profiles must have one or more discontinuities (Altshuller et al., 1987). These are replaced by gradients that more realistically represent axial concentration profiles when finite adsorption rates are incorporated into the model. Numerical simulation of axial concentration profiles for the finite adsorption rate model leads to an understanding of how throughput can be increased without sacrificing product purity and shows that there is an optimum reactor length-feed rate relationship that maximizes throughput.

At feed rates above the optimum the separator floods, and in the dispersionless flow idealization a component that would normally be carried downward with the solids is predicted to move slowly upward until the concentration front moves out of the top of the separator. However, the experimental investigation of the CMCS (Fish et al., 1989) revealed that the front does not move in this way, but becomes stationary above the feed location, with a position that is extremely sensitive to the feed rate. This discrepancy was suggested to be due to the broadness of the experimentally observed front compared with

the concentration discontinuity of the dispersionless model. Here, we employ a finite mass-transfer model that broadens the front. The steady-state model predicts stationary fronts, in good agreement with experiment, but shows that extremely small perturbations in the feed rate will cause movement of the concentration front that can spoil the separation.

Mathematical Model

The component mole balance in an isothermal CMCS, with the assumptions of one-dimensional flow of solids and gas, solid-gas adsorption equilibrium, and neglect of axial dispersion, is given by:

$$\epsilon \frac{\partial C_i}{\partial t} + (1-\epsilon)\frac{\partial n_i}{\partial t} + \epsilon U_g \frac{\partial C_i}{\partial x} - (1-\epsilon)U_s \frac{\partial n_i}{\partial x} = 0 \qquad (1)$$

where C_i and n_i are the gas- and solid-phase concentration, respectively, of the ith component. When adsorption is described by a Langmuir isotherm,

$$\frac{n_i}{N} = \frac{K_i C_i}{1 + \Sigma K_i C_i}, \qquad (2)$$

the method of characteristics can be employed to show that the net speed of a single adsorbable chemical species is given by (Fish et al., 1989):

$$V_i = \frac{U_g\left(1 - \dfrac{\sigma_i}{1+\gamma_i}\right)}{1 + \dfrac{k_i}{1+\gamma_i}} \qquad (3)$$

where $\gamma_i = KC_i$, $k_i = (1-\epsilon)\epsilon^{-1}NK_i$, and $\sigma_i = \epsilon(1-\epsilon)^{-1}\{U_s/U_g\}NK_i$. From Eq. 3 it is apparent that V_i can be either positive or negative, depending on whether $\sigma_i/(1+\gamma_i)$ is less than or greater than one, respectively. In the former case the species moves up the column, and in the latter it moves down. It is also apparent that the direction of movement is concentration-dependent, since a downward moving species ($\sigma_i > 1$) will reverse direction when the concentration becomes large enough to make $\sigma_i/(1+\gamma_i) < 1$. This condition is referred to as flooding. With a binary mixture, the values of U_g, U_s, NK_i, and γ_i can usually be selected so that one component moves up the column, the other down, and a very good separation is obtained. For a linear isotherm, if $\sigma_i > 1$, component i always moves down the column, regardless of the vapor-phase concentration.

Flooding by the more strongly adsorbed component that may occur upon an increase in the feed flow rate, spoiling a separation can be counteracted by increasing the solid flow rate to provide a larger downward flux. This, in turn, may permit further increases in the feed rate, but a limit is reached when the more weakly adsorbed component starts moving down due to increases in U_s (that is, σ_i). At this point there is no longer a separation.

It is desirable to operate the CMCS so that maximum throughput of feed can be obtained without sacrificing separation. The results inferred above from the mole balance will be examined in more detail below to investigate the optimization of CMCS performance.

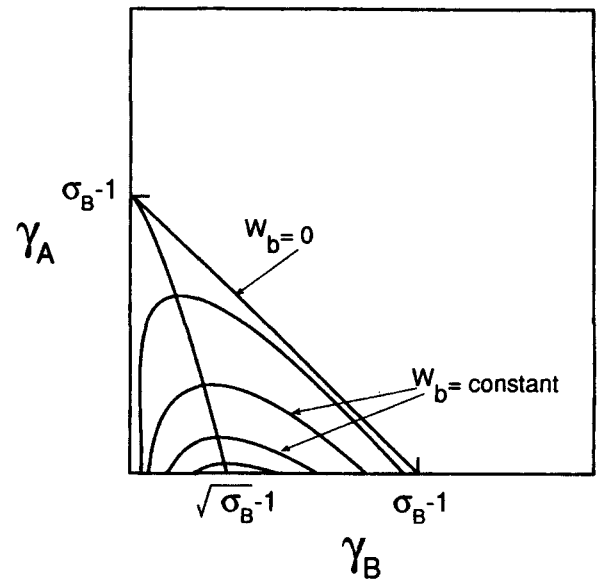

Figure 1. Curves of constant downward flux of species B in the (γ_A γ_B) phase plane for the case σ_A, $\sigma_B > 1$.

Phase Plane Analysis

In the following analysis, a binary feed consisting of components A and B is introduced at a specified side location, and B is assumed to be more strongly adsorbed than A. The concentration of each component depends on the gas-solid partitioning, which is taken to rapidly achieve equilibrium. In steady operation, no accumulation occurs in the column at the feedpoint, and the flux of a component moving upward above the feed, plus the flux moving downward below the feed, must equal the feed rate divided by the column area.

The net flux of component B in a binary mixture is given by:

$$f_B = \epsilon U_g C_B - (1-\epsilon)U_s n_B = \epsilon U_g C_B\left(1 - \frac{\sigma_B}{1+\gamma_A+\gamma_B}\right) \qquad (4)$$

A similar equation can be written for the flux of A. The quantity W_B, proportional to the flux, is defined by:

$$W_B = \frac{f_B K_B}{\epsilon U_g \sigma_B} = \frac{\gamma_B}{\sigma_B} - \frac{\gamma_B}{1+\gamma_A+\gamma_B} \qquad (5)$$

The net flux of B will be positive when $1 > \sigma_B/(1+\gamma_A+\gamma_B)$, and negative when $1 < \sigma_B/(1+\gamma_A+\gamma_B)$. Similar conclusions hold for component A. When $W_B = 0$, then $\sigma_B = 1+\gamma_A+\gamma_B$. This is a straight line with slope -1 and intercepts $\sigma_B - 1$ in the γ_A, γ_B phase plane, as shown in Figure 1. Component B has a downward flux to the left of this line and an upward flux to the right. Lines of constant flux have extrema, as shown in Figure 1 and the extrema can be computed by Eq. 6, which is obtained by setting the derivative of W_B with respect to γ_B at constant γ_A equal to zero:

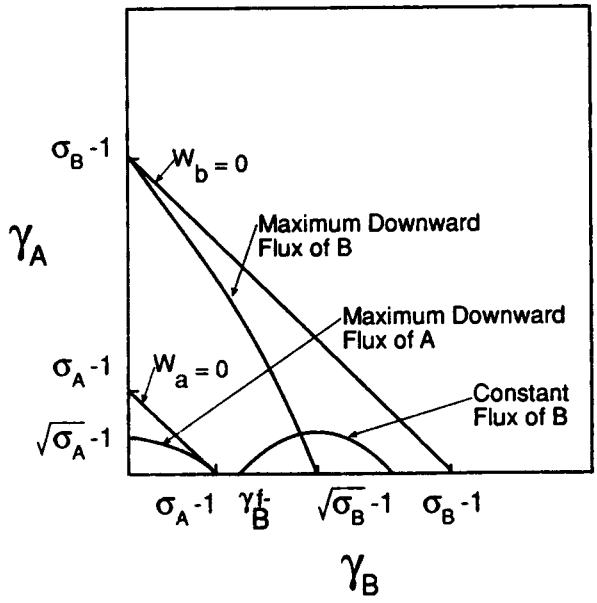

Figure 2. $(\gamma_A\ \gamma_B)$ **phase plane for** $\sigma_B > \sigma_A > 1$ **and** $\sigma_A - 1 < \gamma_B^{f-} < \sqrt{\sigma_B} - 1$.

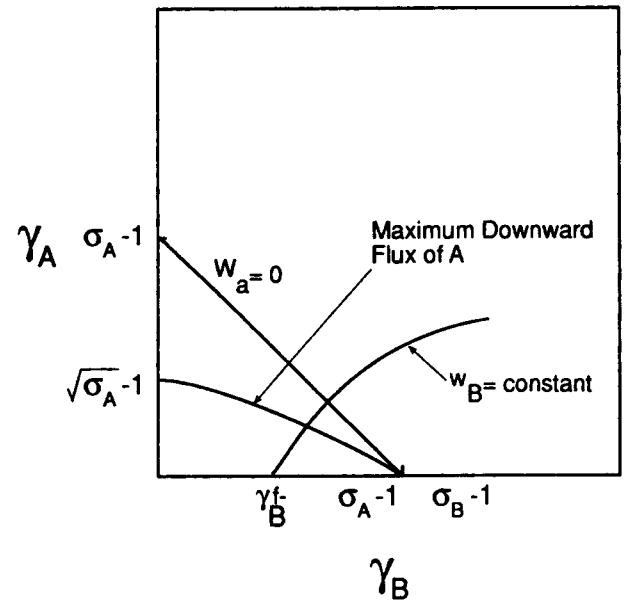

Figure 3. $(\gamma_A \gamma_B)$ **phase plane for** $\sigma_B > \sigma_A > 1$ **and** $\gamma_B^{f-} < \sigma_A - 1$.

$$\gamma_B = -(1+\gamma_A) + \sqrt{\sigma_B(1+\gamma_A)} \tag{6}$$

The locus of the extrema is plotted in Figure 1. Also indicated are the intercepts at $\gamma_A = 0$, $\sqrt{\sigma_B} - 1$, and at $\gamma_B = 0$, $\sigma_B - 1$. Along the locus, component B has the maximum downward flux for a specified γ_A.

When $\sigma_B/(1+\gamma_A+\gamma_B) > 1$, Eq. 4 predicts that the net flux of component B will be downward. An examination of the phase plane reveals the conditions at which A will flow upward and yield a separation even when $\sigma_A > 1$. Consider a column fed with pure B at a rate such that $\sigma_A - 1 < \gamma_B^{f-} < \sqrt{\sigma_B} - 1$. Here, γ_B^{f-} is the concentration of B just below the feedpoint, and it is the starting point of a constant W_B curve that must exist below the feedpoint, since $\sigma_B > 1$ and no B moves up in the nonflooded situation. Figure 2 illustrates that the line $W_A = 0$ lies to the left of $W_B = 0$ at these conditions. If component A is now added to the feed stream and the concentration of B is unchanged, the values of γ_A and γ_B below the feedpoint must lie on the constant W_B line in Figure 2. This region of the phase plane lies to the left of $W_A = 0$ and corresponds to a positive net flux of A. Thus, a product stream of pure A can be removed at the top of the CMCS. In physical terms, component B has occupied a large fraction of the adsorption sites on the solid and decreased its capacity for A. Even though $\sigma_A > 1$, and A is distributed below the feedpoint, the net flux is upward because $\sigma_A/(1+\gamma_A+\gamma_B) < 1$. Since σ_A is independent of γ_A, separation of A from B can be achieved at any concentration of A for the specified feed rate of B. The phase plane clearly shows that this situation will hold for all B feed rates yielding γ_B^{f-} to the right of $\sigma_A - 1$ when $\gamma_A = 0$.

If the feed rate of B is now decreased so that $\gamma_B^{f-} < \sigma_A - 1$, all other conditions remaining the same, the W_B = constant line intersects $W_A = 0$, as shown in Figure 3. It is apparent that the flux of A may be negative at low γ_A (to the left of $W_A = 0$) or positive at higher γ_A. Thus, for small feed rates, A is transported downward and no separation is obtained. As the feed rate of A is increased while maintaining the B feed rate, the flux of A will ultimately become positive, since γ_B is constrained to move along W_B = constant, and separation will occur. This corresponds to displacement of B from the adsorbate by competitive adsorption of A and eventual flooding by A.

The above analysis holds for $\sigma_A - 1 < \sqrt{\sigma_B} - 1$. Another case is obtained from the inequality $\sigma_A - 1 > \sqrt{\sigma_B} - 1$. This situation arises by increasing U_s and produces the phase plane of Figure 4. The behavior of γ_A can be understood by commencing with a feed of pure B such that γ_B^- obtains just under the feedport. Now, if A is introduced at a low rate, it is clear that since γ_A, which is at the intersection of a W_A = constant curve with the W_B = constant shown in Figure 4, lies to the left of $W_A = 0$,

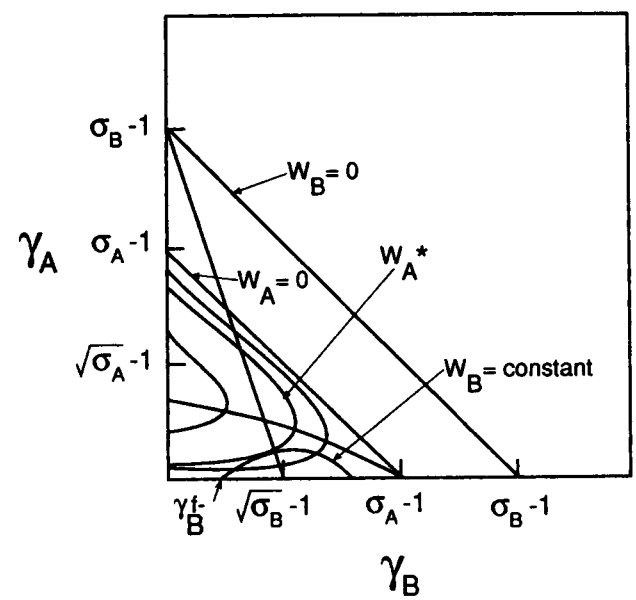

Figure 4. $(\gamma_A\ \gamma_B)$ **phase plane for** $\sigma_B > \sigma_A > 1$ **and** $\sigma_A - 1 > \sqrt{\sigma_B} - 1$.

the flux of A is negative. If the A feed rate is increased at constant B feed rate, γ_A will move upward along W_B = constant until a point of tangency with one of the W_A = constant curves is reached. Movement beyond the point of tangency, along W_B = constant, would correspond to decreasing flux of A with increasing feed rate. This physically unrealistic situation becomes resolved by flooding of the column by component A, causing γ_A above the feedpoint to become greater than $\sigma_A - 1$ by whatever value is required by the mass balance. The concentration of A and B beneath the feedpoint will remain as the coordinates of point N for the greater A feed rates. This behavior is similar to the single-component case, where the maximum downward flux corresponds to vertical characteristics (Fish et al., 1989). Here, it can be shown that the locus of points of tangency of W_A = constant and W_B = constant is a vertical characteristic for the two-component system of equations. In this case, some component A is always lost at the bottom, adsorbed on the solids, due to the large U_s.

Next, we consider the operation of CMCS such that maximum throughput is attained without sacrificing product purity. For the case $\sqrt{\sigma_B - 1} > \sigma_A - 1$, as illustrated in Figure 2, good separations can be obtained with large B feed rates. The B feed rate must give γ_B^f between $\sigma_A - 1$ and $\sqrt{\sigma_B - 1}$. As the solids flow rate is increased, $\sigma_A - 1$ approaches $\sqrt{\sigma_B - 1}$, and the range of B rates for separation decreases. An upper limit for U_s is reached when $\sigma_A - 1 = \sqrt{\sigma_B - 1}$. This results in a maximum of σ_A given by $\sigma_A^{\max} = K^{-1}$. But here, there is only one B rate permitting complete separation, and the separation again would be sensitive to fluctuations in the B rate. In real CMCSs, how closely $\sigma_A - 1$ can approach $\sqrt{\sigma_B - 1}$ without losing separation depends on nonidealities and the length of separator above and below the feed point. This is illustrated in numerical simulations of a CMCS in which concentration fronts are broadened by finite mass-transfer rates.

Numerical Simulation

The fine particles employed in the CMCS experiments (Fish et al., 1989) minimize the effects of intraparticle diffusion, and as is common in gas chromatography, external mass transfer to the stationary phase becomes the dominant resistance and the primary dispersion mechanism (Karger et al., 1973). A mathematical model incorporating finite mass-transfer rates was developed. This has the advantage that discontinuities associated with dispersionless models (Altshuller et al., 1987) are avoided by broadening the concentration fronts. This facilitates numerical simulation and provides realistic axial concentration profiles. The model equations are:

$$-\epsilon U_g \frac{dC_B}{dx} - k_v a (C_B - C_B^*) = 0 \tag{7}$$

$$-\epsilon U_g \frac{dC_A}{dx} - k_v a (C_A - C_A^*) = 0 \tag{8}$$

$$(1-\epsilon) U_s \frac{dn_B}{dx} - \epsilon U_g \frac{dC_B}{dx} = 0 \tag{9}$$

$$(1-\epsilon) U_s \frac{d}{dx}(n_A + n_B) + k_v a (C_B - C_B^*) + k_v a (C_A - C_A^*) = 0 \tag{10}$$

where C_A^* and C_B^* are the gas-phase concentrations just at the surface of the solid phase. The boundary conditions are $C_A = C_B = 0$ at $x = 0$, and $n_A = n_B = 0$ at $x = x^t$. The vapor-phase feed enters at an arbitrary point between $x = 0$ and $x = x^t$ at a rate such that the total gas flow is the same above and below the feed point. It produces a gas-phase concentration discontinuity at the feed point, but the solid-phase concentration is continuous.

If adsorption is rapid enough that C_A^* and C_B^* are in equilibrium with the solid and adsorption follows the Langmuir isotherm, the dimensionless model equations are:

$$-\frac{d\gamma_B}{dz} = St\left(\gamma_B - \frac{\nu_B}{(1-\nu_A-\nu_B)}\right) \tag{11}$$

$$-\frac{d\gamma_A}{dz} = St\left(\gamma_A - \frac{\nu_A}{(1-\nu_A-\nu_B)}\right) \tag{12}$$

$$\sigma_B \frac{d\nu_B}{dz} - \frac{d\gamma_B}{dz} = 0 \tag{13}$$

$$\frac{d}{dz}(\nu_A + \nu_B) = -\frac{St}{\sigma_B}\left(\gamma_B - \frac{\nu_B}{(1-\nu_A-\nu_B)}\right) - \frac{St}{\sigma_B K}\left(\gamma_A - \frac{\nu_A}{(1-\nu_A-\nu_B)}\right) \tag{14}$$

This set of equations was solved by a parallel shooting method (Keller, 1968) employing a first-order continuation on the initial estimates of A and B concentrations at $x = 0$. This gives satisfactory results for $\sigma_B < 2$, but for larger values, the solution becomes more difficult. Figure 5 shows gas-phase axial concentration profiles for a range of B feed rates at $\sigma_B = 2.2$. The position of the B front above the feed is very sensitive to the feed rate. A change in the dimensionless B feed rate of only 0.008 moves the front from just above the feedpoint nearly to the reactor exit. This sensitivity of concentration profiles of a species that would be confined to the length of column below the feed at low feed rates, but is carried above it when flooding occurs, has been observed experimentally (Fish et al., 1989). The conditions producing these profiles, with B distributed both above and below the feedpoint and A only above it, correspond to the phase plane analysis of Figure 2.

When σ_B is increased, the front becomes even more sensitive to the flow rate, requiring extremely small increments to prevent losing convergence. This problem can be circumvented by continuing in some variable other than the feed rate. The approach taken was to continue in the arc length of the solution (Kubicek and Marek, 1983). A fourth-order Adams-Bashforth integration was employed to integrate each step in arc length, iterating for convergence and with step size in arc length adjusted depending on the number of iterations.

Optimization

The conditions that maximize throughput and minimize column length while maintaining specified product stream purity are considered here. One approach to this problem would be to specify the feed composition, feed rate, and purity, and then to calculate the required CMCS length and feed position

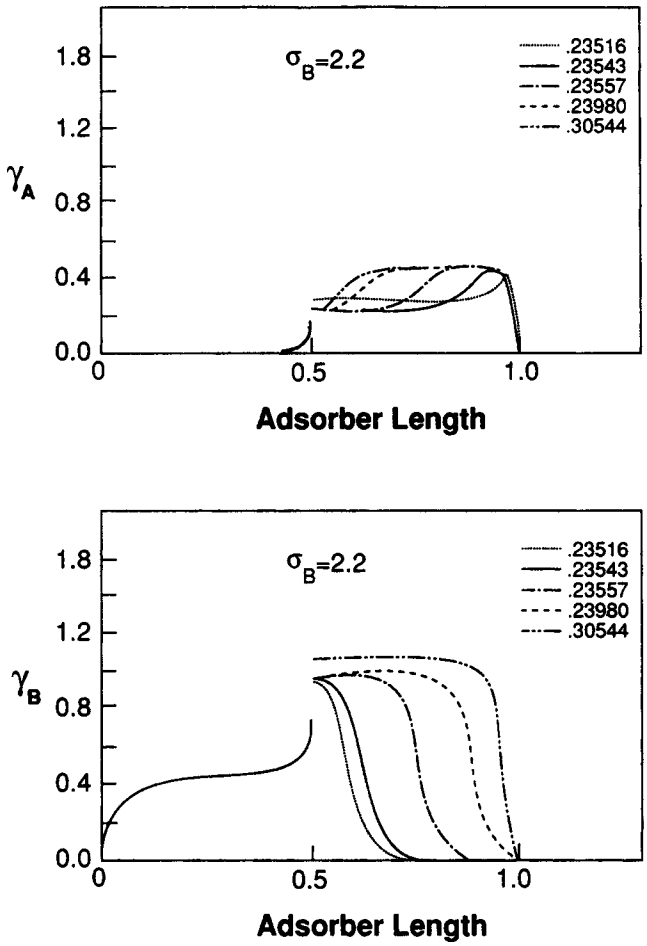

Figure 5. Progression of axial concentration profiles with increasing reactant feed rate.

Feed position, $x=0.5$.

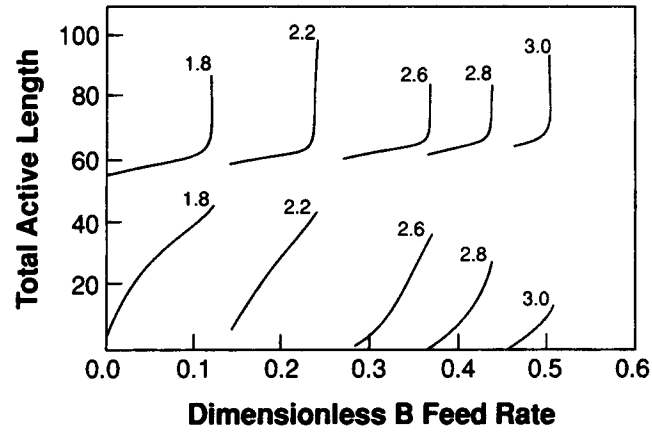

Figure 6. Position at which 98% purity is achieved in the CMCS as a function of reactant feed rate with σ_B as a parameter, $\sigma_B/\sigma_A=2$.

The inlet position is at $x=0.5$.

as a function of operating parameters. A shooting method, in which an initial guess of adsorbed concentrations of A and B at $z=0$ is made, and Eqs. 11-14 are integrated up to the feedpoint, where the feed conditions are applied and then the integration continued to the top of the CMCS requires much computation. The solution to match the top boundary condition, $\nu_A=\nu_B=0$, would first have to be iterated for a given feed position and column length, followed by iterations on length and feed position to satisfy the required A and B product purity.

A simpler approach was implemented by assuming that CMCS is long enough for complete separation. Since most of the mass transfer occurs near the feedpoint and increasing column length changes feedpoint concentrations only slightly, it is possible to calculate concentration profiles above and below the feed when the desired product purity is reached. In these calculations, the required purity of the two product streams was specified to be 98%. An "active length" was then defined to be the sum of the distances above and below the feed when 98% purity was attained. The computational advantage is that for a given feed rate one calculation gives the CMCS length for specified purity. It does not give quite the same information as the iterative approach, but it does provide insight into optimization of the CMCS.

All the numerical work employed equimolar feed mixtures, $St=100$, and $K=1/2$. Since the active length depends on the mass-transfer coefficient, the results are presented as fraction of dimensionless length divided by St. According to the results from the phase plane analysis, it is expected that higher throughputs will be obtained when σ_A, $\sigma_B>1$, but as the σ's increase, the range of feed rates from which the required separation can be obtained will be narrow. There should be a maximum value of σ_A and σ_B, above which separation can no longer be achieved.

Results and Discussion

Figure 6 shows the active length, the length required for 98% purity vs. dimensionless feed rate of B when $\sigma_B/\sigma_A=2$. The feedpoint is at $x=0.5$. The curves are not concentration profiles, but correspond to the positions, at a particular feed rate, where the product streams are 98% B (always below the feedpoint) and 98% A (always above the feedpoint). These positions give the optimum separator length for a 98% separation at specified feed rates. For example, when $\sigma_B=1.8$ and the feed rates are very low, the feedpoint should be located toward the top of the separator, which would correspond to a dimensionless length in the vicinity of 0.55 to 0.6. The lower section is required to be longer, with a B takeoff located at about 0.05 to 0.1. As the B feed rate increases, the total active length at first decreases, with the top active length increasing while the bottom decreases more rapidly. At a dimensionless B feed rate somewhat larger than 0.1, the 98% A purity location rapidly moves toward 1.0 with slight increases in the B feed rate, increasing the total active length. However, this is also the region in Figure 5, where B floods the column and very small increments in B feed rate move it out of the top and the separation is lost.

To recover the separation, σ_B must be increased; however, if σ_B is increased beyond 2 the separation is lost again, for maintaining $\sigma_B/\sigma_A=2$ then makes $\sigma_A>1$ and A moves downward. The separation, however, can be recovered if the feed rate is increased. Thus, there is a range of feed rates where separation can be obtained even though $\sigma_A>1$. This range of feed rates decreases as σ_B increases. The ideal reactor model

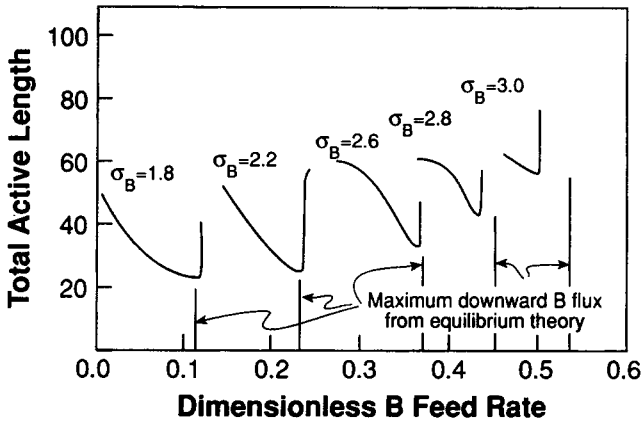

Figure 7. Total active length (for 98% purity) as a function of dimensionless B feed rate when $\sigma_B/\sigma_A = 2$.

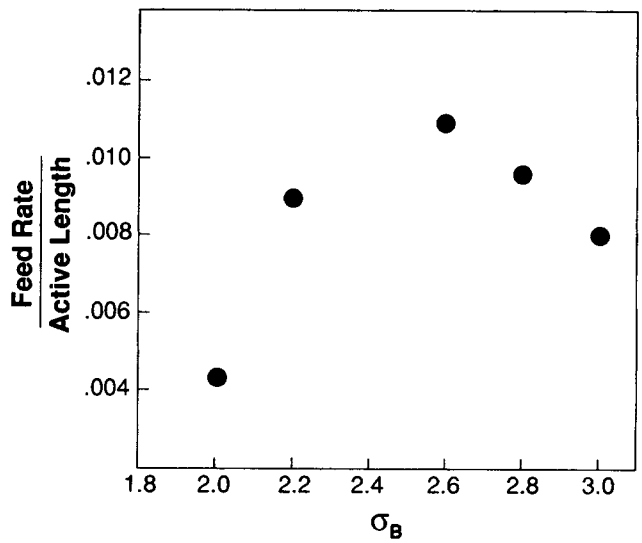

Figure 8. Maximization of feed rate per active length of separator when $\sigma_B/\sigma_A = 2$.

predicts that the maximum value of σ_B above which separation is not possible is 4 if $\sigma_B/\sigma_A = 2$, since $\sigma_A^{max} = K^{-1}$ (see above) and $K = 1/4$ in these simulations. Separation was not obtained in calculations with $\sigma_B = 3.5$, most probably because of the nonideality introduced by the incorporation of finite mass-transfer rates into the model. Larger values of St would presumably predict separation when $3.5 < \sigma_B < 4$.

In Figure 7 the total active length, which is the distance between the 98% points of Figure 6, is plotted vs. dimensionless B feed rate for a range of σ_B at $\sigma_B/\sigma_A = 2$. For each value of σ_B, the active length decreases with increasing B feed rate until a minimum, the optimal solution for the stated conditions, is reached. Beyond the optimum, only slight increases in the B feed rate cause B to flow upward and spoil the separation. Thus, operation at the optimum may be difficult since disturbances in the B feed rate will cause fluctuations in product purity. An increase may send B up the column to become mixed with A at the top product take-off, while a decrease will require a longer column for 98% separation, and both A and B purity will deteriorate.

Figure 8 shows the ratio of feed rate to active length vs. σ_B, revealing, in the approximate range of $2.2 < \sigma_B < 2.8$, the existence of a maximum which optimizes the separation. Larger feed throughputs can be handled at larger σ_B, but a longer separator must be used. Also, the range of feed rates which allows separation decreases as σ_B increases.

Also plotted on Figure 7 is the maximum feed rate permitted by the ideal model (equilibrium theory) before flooding. At the lower range of σ_B this is only slightly less than the maximum rate predicted by the nonequilibrium model, which is located at the rapid upturn in active length. At the low end of the feed rate range the nonideality introduced by the finite mass-transfer model has very little effect on the flooding characteristics, perhaps because the B component profile is relatively flat beneath the feedpoint (see Figure 5), and the gas-solid distribution of B approaches equilibrium. Thus, the flux of B will approach the equilibrium theory prediction. At the high end of the σ_B range, the feed rate at flooding is significantly less than the equilibrium model prediction due to the influence of end effects. Here, the mass-transfer zone for A extends farther below the feedpoint, and A competes with B for adsorption. This gives rise to smaller downward fluxes of B than predicted by equilibrium theory, and component B flooding at lower feed-rates.

Summary

The net flux of a component in a CMCS depends on the quantity $\sigma/(1+\Sigma\gamma)$. When this is less than unity, the flux is negative and the component is carried downward; when it is greater than unity, the flux is positive and the component moves upward. Separations become possible when $\sigma/(1+\Sigma\gamma)$ is greater than one for one component or a group of components, and less than one for the other. At very low feed rates, when $\Sigma\gamma \ll 1$, the fluxes depend on whether σ is greater than or less than unity. It is readily seen that a component with a net upward flux at low feed rate continues to move upward as feed rate, hence mobile-phase concentration, increases, while a component with a net downward flux at low feed rate may go over to a net upward flux at high feed rate. The phase plane approach employed here permits an analysis of when binary separations are expected based only on the parameter σ, since mobile-phase concentrations are difficult to obtain and vary widely along the separator axis. It has the advantage that only the adsorption equilibrium constant and the bed voidage need be known, along with measurement of the solid- and mobile-phase flow rates. For two components, A and B, separation will always be obtained if $\sigma_A < 1$ and $\sigma_B > 1$, or vice versa. To increase productivity the feed rate must be increased, and the analysis shows that for large B feeds, $\sigma_A > 1$, $\sigma_B > 1$, and $\sigma_A - 1 < \gamma_B^{f-} < \sqrt{\sigma_B} - 1$ gives the conditions for separation. When $\sigma_A - 1$ approaches $\sqrt{\sigma_B} - 1$, separations are extremely sensitive to the B feed rate. The feed rate sensitivity is detailed in numerical simulations of CMCS performance by means of a mathematical model incorporating finite rates of mass transfer to adsorbent granules.

The conclusions of the phase plane analysis and the simulations are corroborated by a previously published experimental investigation of the separation of 1,3,5-trimethylbenzene or mesitylene(MES), and 1,3,5-trimethylcyclohexane, TMC

(Fish et al., 1989). With $\sigma_{MES} > 1$ and $\sigma_{TMC} < 1$, at low feed rates it was observed that MES was carried downward and TMC upward from the feed position midway along the CMCS, in accord with theoretical predictions. Top and bottom product streams of high-purity TMC and MES, respectively, were obtained. At higher feed rates, flooding by MES occurred, as stationary MES concentration fronts above the feed were observed, but good separations still obtained. Their position was very sensitive to the feed rate, small increases causing the MES front to exit the top of the SCMCS, spoiling the separation. This observation is in accord with the results of the numerical simulations, with their broadened concentration fronts and in contrast with the predictions of dispersionless models where the concentration discontinuity under flooding is not predicted to become stationary, but to slowly move up and out of the column.

Acknowledgment

This work was supported by the Division of Chemical Sciences, Office of Basic Energy Sciences, U.S. Department of Energy, under contract No. DE-AC02-76-ER02945.

Notation

a = area for mass transfer per bed volume
C_i = gas-phase concentration of component i
f = net molar flux
k = $[(1-\epsilon)/\epsilon]NK$
k_v = mass-transfer coefficient
K = $\sigma_B/\sigma_B = K_A/K_B$
K_i = adsorption equilibrium constant of component i
n_i = solid-phase concentration of component i
N = solid-phase saturation concentration
S_t = Stanton number, $k_v aL/\epsilon U_g$
t = time
W_i = $f_i K_i/\epsilon U_g \sigma_i$
U_g = carrier fluid speed
U_s = solid-phase speed
x = axial distance
z = dimensionless axial length, x/L
$[\ ]^f$ = quantities just below the feed location
$[\ ]^t$ = quantities just inside the top of the separator
$[\ ]^t$ = quantities just outside the top of the separator

Greek letters

γ_i = $C_i K_i$, dimensionless gas-phase concentration
ϵ = interparticle void fraction
ν_i = n_i/N, dimensionless solid-phase concentration
σ_i = $[(1-\epsilon)/\epsilon](U_s/U_g)NK_i$

Literature Cited

Altshuller, D., G. Vazquez, R. Aris, and R. W. Carr, "An Analysis of a Countercurrent Adsorber," *Chem. Eng. Comm.*, **52**, 311 (1987).
Barker, P. E., and G. Ganetsos, *Sep. Sci. Technol.*, **22**, 2011 (1987).
Barker, P. E., and G. Ganetsos, *Adsorption: Science and Technology*, A. E. Rodrigues et al., eds., Kluwer Academic Publishers, p. 471 (1989).
de Rosset, A. J., R. W. Neuzil, and D. B. Broughton, *Percolation Processes: Theory and Applications*, A. E. Rodrigues and D. Tondeur, eds., NATO Advanced Study Institutes Series, **33**, 249 (1981).
Fish, B. B., R. W. Carr, and R. Aris, "The Continuous Countercurrent Moving Bed Separator," *AIChE J.*, **35**, 737 (1989).
Karger, B. L., L. R. Snyder, and C. Horvath, *An Introduction to Separation Science*, Wiley-Interscience, 135 (1973).
Keller, H. B., *Numerical Methods for Two-Point Boundary Value Problems*, Blaisdell, London (1968).
Kubicek, M., and M. Marek, *Computational Methods in Bifurcation Theory and Dissipative Structures*, Springer-Verlag (1983).
Ruthven, D. M., *Principles of Adsorption and Adsorption Processes*, Wiley Interscience, 380 (1984).

Manuscript received Aug. 31, 1992, and revision received Feb. 2, 1993.